A&A, 708, A281 (2026)
https://doi.org/10.1051/0004-6361/202658985

Astronomy & Astrophysics

C_5H_6 formation in Dense Molecular Clouds

Ugo Jacovella[1,⋆], Jean-Christophe Loison[2,⋆], Corentin Rossi[1], Anne P. Rasmussen[1,3], Roland Thissen[4,5], Nandana Pattathadathil[4,6], and Christian Alcaraz[4]

[1] Université Paris-Saclay, CNRS, Institut des Sciences Moléculaires d'Orsay, 91405 Orsay, France
[2] Université Bordeaux, CNRS, Bordeaux INP, ISM, UMR 5255, 33400 Talence, France
[3] Department of Physics and Astronomy, Aarhus University, Ny Munkegade 120, 8000 Aarhus C, Denmark
[4] Université Paris-Saclay, CNRS, Institut de Chimie Physique, UMR8000, 91405 Orsay, France
[5] Synchrotron SOLEIL, L'Orme des Merisiers, 91192 Saint Aubin, Gif-sur-Yvette, France
[6] Department of Physics, University of Trento, Via Sommarive 14, 38123 Trento, Italy

Received 15 January 2026 / Accepted 16 February 2026

ABSTRACT

Context. Cyclopentadiene (C_5H_6) has been recognized as a crucial precursor in the formation of nonplanar polycyclic aromatic hydrocarbons (PAHs) and carbon-rich nanostructures in space. Despite its significance and detection in the Taurus Molecular Cloud (TMC-1), the elementary gas-phase reaction pathways leading to cyclopentadiene from acyclic hydrocarbon precursors remain poorly constrained. This gap is emphasized by persistent discrepancies between astrochemical model predictions and the abundances inferred from its radioastronomical detection.

Aims. The aim of this work is to reconcile the chemical network that predicts the formation of C_5H_6 – a key intermediate in the growth of aromatic species – from gas-phase chemistry with its observed abundance in TMC-1.

Methods. We used combined experimental work conducted with the CERISES tandem mass spectrometer at the SOLEIL synchrotron, together with quantum chemical calculations, to determine and refine reaction rate coefficients and branching ratios for reaction pathways that lead to the formation of $C_5H_7^+$. We then incorporated these results into the gas–grain chemical code NAUTILUS to model the formation of C_5H_6.

Results. We identify the reactions $C_2H_4^+ + CH_3CCH$ and $C_3H_7^+ + C_2H_2$ as an important source of $C_5H_7^+$ and, consequently, of C_5H_6 in TMC-1. We experimentally determined the $C_2H_4^+ + CH_3CCH$ reaction rate to be 1×10^{-9} cm^3 s^{-1}. In addition, the radiative association reactions C_4H_5 + H and C_5H_5 + H under low-pressure conditions deserve further investigation, as they may constitute key intermediate steps in the formation of C_5H_6 through neutral–neutral reaction pathways.

Conclusions. Our updated chemical model accounts for several previously missing formation pathways of C_5H_6. Although it reproduces only ∼20% of the observed abundance, this represents a significant improvement compared to existing models. We identify the reactions $C_2H_4^+ + CH_3CCH$ and $C_3H_7^+ + C_2H_2$ as the two dominant sources of $C_5H_7^+$. However, the formation of C_5H_6 through neutral–neutral chemistry remains poorly constrained. The main source is the radiative association of C_5H_5 + H but 1,3-butadiene (C_4H_6) appears to be a key intermediate in the formation of C_5H_6; however, its abundance is uncertain due to the disputed detection of its cyano-derivative proxy. Further work is therefore required to better constrain the abundance of 1,3-butadiene, which may be efficiently formed through the radiative association C_4H_5 + H.

Key words. astrochemistry – methods: laboratory: molecular – ISM: abundances – ISM: molecules – ISM: individual objects: TMC-1

1. Introduction

Cold molecular clouds, exemplified by the Taurus Molecular Cloud (TMC-1), have long been regarded as prime astrophysical environments for probing molecular mass growth on macroscopic scales. Through the combination of high-sensitivity astronomical observations and astrochemical modeling based on extensive gas-phase reaction networks involving ion–molecule and neutral–neutral processes, these regions provide unique insights into the formation pathways of complex molecules.

Following the detection of cyclic C_3H_2 by Thaddeus et al. (1985), decades of sustained effort have been devoted to the identification of aromatic and cyclic hydrocarbons in the interstellar medium (ISM), with particularly significant success achieved only recently in the cold dark cloud TMC-1. This advancement has been driven by large observational programs—most notably the QUIJOTE and GOTHAM surveys—which have played a key role in substantially expanding the known inventory of cyclic hydrocarbons in space. These efforts have resulted in the detection of a wide variety of nonaromatic and aromatic species, including ethynyl cyclopropenylidene (C_3HCCH), cyclopentadiene (C_5H_6), and indene (C_9H_8) in Cernicharo et al. (2021a), ethynylbenzene (C_6H_5CCH) by Loru et al. (2023), o-benzyne (o-C_6H_4) by Cernicharo et al. (2021b), fulvenallene ($C_5H_4CCH_2$) by Cernicharo et al. (2022), and phenalene ($C_{13}H_{10}$) by Cabezas et al. (2025).

In addition, numerous cyano derivatives have been identified, including species whose hydrocarbon counterparts are undetectable, as well as derivatives of already detected cyclic molecules. Notable examples include benzonitrile (C_6H_5CN) by McGuire et al. (2018), cyanocyclopentadiene (C_5H_5CN) by McCarthy et al. (2021), cyanonaphthalene ($C_{10}H_7CN$) by McGuire et al. (2021), cyanoindene (C_9H_7CN) by Sita et al. (2022), cyanoacenaphthylene ($C_{12}H_7CN$) by

⋆ Corresponding authors: ugo.jacovella@cnrs.fr; jean-christophe.loison@cnrs.fr

Cernicharo et al. (2024), cyanopyrene ($C_{16}H_9CN$) by Wenzel et al. (2024), and cyanocoronene ($C_{24}H_{11}CN$) by Wenzel et al. (2025). Many of these molecules exhibit relatively high fractional abundances, reaching up to 10^{-8} with respect to molecular hydrogen, which has fueled growing interest in the elementary chemical mechanisms that drive the conversion of acyclic hydrocarbons into cyclic species and, ultimately, polycyclic aromatic hydrocarbons (PAHs).

Within this molecular inventory, C_5H_6 occupies a pivotal role. It serves as a key precursor to five-membered-ring-containing aromatic molecules such as indene (C_9H_8), which themselves are fundamental structural units in the formation of bowl-shaped aromatic hydrocarbons and carbon cages. Consequently, any comprehensive description of molecular mass growth toward nonplanar aromatic systems must begin with a detailed understanding of how cyclopentadiene is synthesized from simpler, acyclic precursors.

Despite its detection in TMC-1, robust gas-phase formation mechanisms for cyclopentadiene remain poorly constrained. As a result, current classical ion-molecule-based astrochemical models significantly underpredict its abundance, by several orders of magnitude, relative to astronomical observations (Cernicharo et al. 2021a; Mallo et al. 2025). This discrepancy highlights a critical gap in our knowledge of synthetic pathways to cyclopentadiene under interstellar conditions. Identifying and characterizing the missing pathways is therefore essential for advancing our understanding of molecular mass growth in cold clouds and for elucidating the chemical evolution leading to complex PAHs that could ultimately lead to carbonaceous dust grains.

Two distinct formation pathways have been proposed for C_5H_6. The most recent involves a nonclassical neutral–neutral chemistry developed by Yang et al. (2024). The more conventional pathway proceeds through a sequence of ion–molecule reactions that lead to the protonated precursor $C_5H_7^+$, which subsequently forms C_5H_6 via dissociative recombination (DR), in analogy with the formation of benzene from $C_6H_7^+$ (Loison et al. 2026). However, astrochemical models relying on this latter pathway systematically underestimate the observed abundance of C_5H_6, which likely indicates the absence of one or more key ion–molecule reactions that efficiently produce $C_5H_7^+$, as noted by Mallo et al. (2025).

In contrast, the model based on neutral–neutral chemistry proposed by Yang et al. (2024) appears to approach the observed abundance of C_5H_6. In this model, the dominant pathway is the reaction $CH + C_4H_6 \rightarrow C_5H_6 + H$, where C_4H_6 corresponds to 1,3-butadiene. A significant limitation of this pathway arises from the uncertainty in the abundance of C_4H_6. While the abundance of the CH radical is well constrained by observations, C_4H_6 remains undetected due to its lack of a permanent dipole moment, and its abundance is inferred solely through chemical modeling (Cooke et al. 2023; Agúndez et al. 2025). Moreover, the model of Yang et al. (2024) neglects the reaction of C_4H_6 with atomic carbon, which is expected to represent a major destruction route for C_4H_6 (Husain & Ioannou 1997; Hahndorf et al. 2000), and then the model likely overestimates the C_4H_6 abundance.

In this study, we therefore conducted another exploration of potential ion–molecule reactions leading to $C_5H_7^+$. The most promising candidate reaction was subsequently investigated experimentally, and the resulting new kinetic data were incorporated into the astrochemical model.

2. Methods

2.1. Experimental

We produced parent ions ($C_2H_4^+$) via direct photoionization of ethylene (N35 air liquide) using vacuum ultraviolet (VUV) radiation in the 10.5–12 eV range at the DESIRS beamline of the SOLEIL synchrotron (Saint-Aubin, France). We investigated the reactions using the CERISES apparatus, which is a home-built tandem mass spectrometer coupled to the VUV source (Cunha De Miranda et al. 2015; Rossi et al. 2023). Following mass selection, the parent ions were guided into a reaction cell with a controlled collision energy, and the resulting product ions were analyzed using a second quadrupole. We derived absolute reaction cross sections from the neutral reactant (propyne and allene) pressure and measured ion intensities. The pressure was kept as low as possible (below 100 nbar) to maximize the likelihood of single-collision conditions. We examined the reaction with both C_3H_4 isomers at a fixed center-of-mass collision energy of 0.15 eV, while the internal energy of the parent ions was varied by tuning the photon energy. We determined the rate constants from the absolute reaction cross section measured, following the methodology described in the study of C_3H^+ reactivity by Rossi et al. (2025).

2.2. Astrochemical modeling

We employed a standard astrochemical model using the Nautilus code (Ruaud et al. 2016), which is a three-phase, time-dependent, chemical model that includes the gas phase, the dust-grain ice surface, and the dust-grain ice mantle. The model is based on the kida.uva.2024 reaction network (Wakelam et al. 2024), which has been recently updated to provide an improved description of complex organic molecule (COM) chemistry both on interstellar dust grains and in the gas phase (Manigand et al. 2021; Hickson et al. 2021; Coutens et al. 2022; Hickson et al. 2024). There are 800 individual species included in the network that are involved in approximately 9000 separate reactions. Elements are initially assumed to be in their atomic or ionic forms, and elements that have an ionization potential lower than 13.6 eV are considered to be fully ionized. This assumption reflects the adopted initial abundances at time t = 0 in the evolution of dense clouds, which are taken to correspond to those of a diffuse cloud. In such environments, elements are predominantly in their atomic form, and ultraviolet photons ionize species with ionization potentials below 13.6 eV. The high abundance of atomic hydrogen strongly limits the propagation of photons with energies above 13.6 eV, as these photons are efficiently absorbed by hydrogen atoms. The C/O gas phase elemental ratio is equal to 1 in this work. This value, which is higher than the cosmic abundance ratio (0.6), leads to a significantly better agreement between the model predictions and the full set of observations. For lower C/O ratios, the available carbon is insufficient to bind most of the oxygen into CO, leaving excess oxygen atoms that suppress radical abundances and consequently inhibit the chemistry. This choice is consistent with that adopted in previous studies of aromatic species in dense molecular clouds, including Hincelin et al. (2011), Byrne et al. (2024) and Mallo et al. (2025). Physically, this oxygen depletion is attributed to the formation of water ice during the history of the dense cloud. This water ice remains largely trapped on dust grains and does not desorb during subsequent warmer and less dense phases, in contrast to CO,

which efficiently desorbs and is dissociated into C and O under these conditions (Hincelin et al. 2016; Wakelam et al. 2019). The initial simulation parameters adopted in this work are summarized in Table A.1. The grain surface and the mantle are both chemically active for these simulations, while accretion and desorption are only allowed between the surface and the gas phase. The dust-to-gas ratio (in terms of mass) is 0.01. A sticking probability of 1 is assumed for all neutral species, while desorption occurs by both thermal and nonthermal processes (cosmic rays, chemical desorption), including sputtering of ices by cosmic ray collisions (Wakelam et al. 2021).

2.3. Identification of important reactions

We identified Potential formation routes of C_5H_6 following an approach similar to that adopted in previous studies of Titan's atmospheric chemistry (Hébrard et al. 2012, 2013; Dobrijevic et al. 2014; Loison et al. 2015; Dobrijevic et al. 2016; Loison et al. 2019) and of carbon chemistry in dense molecular clouds (Loison et al. 2013, 2014, 2016, 2017). We focused on the analysis of reactions leading to species directly related to C_5H_6, namely C_5H_5, C_5H_6, and $C_5H_7^+$, and restricted to pathways involving species detected or predicted to have significant modeled abundances. We considered both ion–molecule and neutral–neutral reactions. For ionic chemistry, we examined systems of the type $CH_x^+ + C_4H_y$, $C_2H_x^+ + C_3H_y$, and related reactions, together with neutral reactions such as $CH_x + C_4H_y$. Species with negligible abundances, notably CH^+ and CH_2^+, which are rapidly removed by reactions with H_2, were excluded as potential precursors of aromatic C_5H_6. Once a comprehensive list of reactions that potentially produce C_5H_5, C_5H_6, and $C_5H_7^+$ had been compiled, we conducted an extensive bibliographic search for each reaction. When reaction rate coefficients had been measured, at least at room temperature, and were found to be larger than 10^{-11} cm^3 s^{-1}, these reactions were assumed to be barrierless and therefore efficient under dense molecular cloud conditions. For many reactions, no experimental or theoretical data were available. In such cases, reactions that could plausibly be fast at low temperatures were first identified and we systematically investigated the presence of activation barriers by searching for transition states (TS) using density functionnal theory (DFT) calculations performed using the Gaussian 16 software package (Frisch et al. 2016). We employed the M06-2X functional with the cc-pVTZ basis set. This highly nonlocal functional, developed by Zhao & Truhlar (2008), is well suited for describing transition-state structures and energetics. However, the absence of a located TS does not necessarily imply the absence of an activation barrier. Reactions for which no TS was found were therefore compared with analogous, well-characterized reactions. For example, we assumed that if a species reacts with C_2H_2, it is also likely to react with other alkynes, and similarly that reactivity with C_2H_4 implies reactivity with alkenes. For reactions considered barrierless, we determined or estimated reaction products and branching ratios. When experimental data were unavailable, we used existing theoretical studies when possible. In the absence of any prior information, we performed additional DFT calculations to characterize key intermediates, allowing likely products and branching ratios to be estimated. It should be noted that, given the number of atoms involved and the excess energy available in these systems, a very large number of intermediate species may be formed. The present approach does not aim to identify all possible intermediates, which would require detailed, reaction-specific studies, such as those performed for the l–$C_3H_3^+ + C_2H_4$ reaction by Mallo et al. (2025). Instead, we assess the feasibility of cyclization and the formation of aromatic compounds.

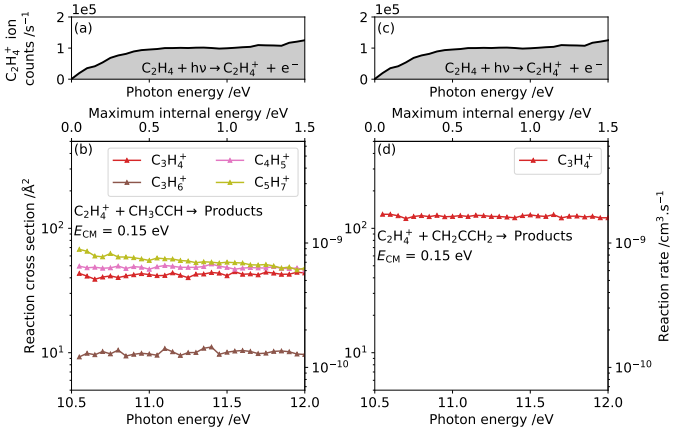

Fig. 1. Panels a and c display the $C_2H_4^+$ parent-ion signal from the photoionization of ethylene. Panels b and d show the reaction cross sections (left axis) and rate constants (right axis) with propyne and allene, respectively, as a function of photon energy.

3. Experimental investigation of the reaction $C_2H_4^+ + C_3H_4$

Once the reaction of $C_2H_4^+$ with propyne was identified as a potentially important chemical route to $C_5H_7^+$, we decided to experimentally investigate its reaction rate and branching ratio as a function of internal energy. Although allene is not directly detected due to its lack of a permanent dipole moment, it is assumed to be as abundant as propyne in TMC-1. We therefore investigated the reaction of $C_2H_4^+$ with both C_3H_4 isomers.

Panels b and d in Figure 1 present the reaction cross sections (left axis) and rate constants (right axis) for reactions with propyne and allene, respectively, as a function of photon energy. Only reaction channels with cross sections exceeding those leading to $C_6H_7^+$ are shown (3 Å^2 and 7 Å^2 at 10.6 eV for reactions with propyne and allene, respectively). The $C_6H_7^+$ signal arises from a secondary process, namely charge transfer followed by the reaction $C_3H_4^+ + C_3H_4$. Since $C_3H_4^+$ is formed via charge transfer with no transfer of momentum, it has a sufficiently long residence time in the reaction cell to undergo secondary reactions with C_3H_4, such that this channel cannot be fully suppressed even at very low pressure. However, all nonreported channels contribute, at maximum, a few percent relative to the dominant product, as can be seen in Fig. B.1. Overall, we observed no significant dependence on photon energy over the explored range. Consequently, the reaction rates reported in Appendix C were taken at the lowest photon energy (10.6 eV), which corresponds to the minimum possible internal energy of the ions.

Three products dominate the reaction with propyne (panel b): the formation of $C_5H_7^+$ (m/z 67), the charge-transfer product $C_3H_4^+$ (m/z 40), and $C_4H_5^+$ (m/z 53). All reaction rates are listed in the table in Appendix C, row 6. In contrast, the reaction with allene predominantly yields the charge-transfer product, with a rate that is more than an order of magnitude higher than the formation of $C_5H_7^+$. Corresponding data are provided in the table in Appendix C, row 7.

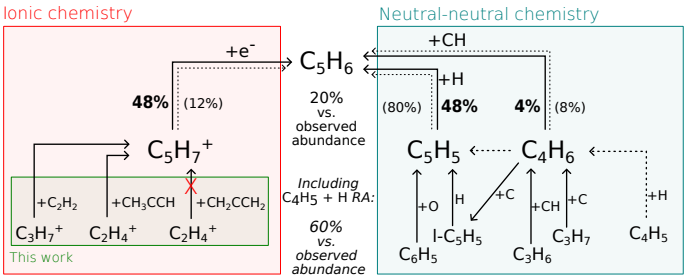

Fig. 2. Schematic diagram showing the main formation routes of C_5H_6 in TMC-1. Percentages written in bold indicate the contribution of the reactions in the nominal model. Percentages in normal text, associated linked with dashed arrows, correspond to their contribution if the C_4H_5 + H reaction is included.

4. Formation of C_5H_6 in TMC-1

Figure 2 summarizes the main formation routes of C_5H_6 in TMC-1. Two comparable contributions are identified in the nominal model: the ion–molecule network and the neutral–neutral chemistry, each accounting for about 50% of the total production based on experimentally measured or theoretically validated rate coefficients. The ionic contribution is dominated by the reactions $C_2H_4^+ + CH_3CCH$ and $C_3H_7^+ + C_2H_2$, which are discussed in detail below. In the neutral network, the dominant source is the radiative association (RA) $C_5H_5 + H$. The alternative pathway $C_6H_4 + CH$, recently proposed by Yang et al. (2024), is reassessed here. The possible indirect role of the RA reaction $C_4H_5 + H$ is also examined. The complete list of reactions considered is presented in the table in Appendix C.

4.1. Ionic chemistry

In the chemical network, ion–molecule chemistry contributes to the formation of C_5H_6 primarily through the production of the precursor ion $C_5H_7^+$, followed by DR. Although no direct measurements of branching ratios for the DR of aromatic ions are currently available, laboratory studies of $C_6D_6^+$ and $C_6D_7^+$ show that the aromatic ring is preserved in more than 90% of events (Hamberg et al. 2011). By analogy, we assume that ring preservation also dominates the DR of $C_5H_7^+$, such that the $C_5H_7^+ + e^-$ reaction predominantly yields $C_5H_6 + H$. A comparison between model predictions and observations of C_5H_6 is shown in Fig. 3, with panel (a) illustrating the relative contribution of ionic chemistry to the overall formation of C_5H_6.

The $C_5H_7^+$ ion is produced mainly through two reactions: $C_2H_4^+ + CH_3CCH$, which has been studied both here and previously (Anicich et al. 2006), and $C_3H_7^+ + C_2H_2$. To date, no dedicated experimental or theoretical investigation of the latter reaction has been reported. However, it is isoelectronic with $C_3H_5^+ + C_2H_4$ (Anicich et al. 2003, 2006; McEwan et al. 1998) and exhibits similar exothermicities, which suggests that it is a viable and potentially efficient source of $C_5H_7^+$. Preliminary calculations performed in this work indicate that the $CH_3CH_2CH_2^+$ isomer reacts with C_2H_2 to form $C_5H_7^+ + H_2$, which supports this interpretation and highlights the need for more detailed studies. Several additional formation routes to $C_5H_7^+$ were identified. Some are experimentally well characterized, including $C_2H_5^+ + CH_3CCH/CH_2CCH_2$ (Lifshitz et al. 1981), $C_3H_4^+ + C_2H_4$ (McEwan et al. 1998; Anicich et al. 2006), and $C_3H_5^+ + C_2H_4$ (Anicich et al. 2003, 2006; McEwan et al. 1998). Other plausible contributors include $CH_3^+ + CH_2CHCHCH_2$, $C_2H_3^+ + C_3H_6$, $C_3H_6^+ + C_2H_2$, and $C_4H_3^+ + C_3H_6$, although these remain poorly constrained.

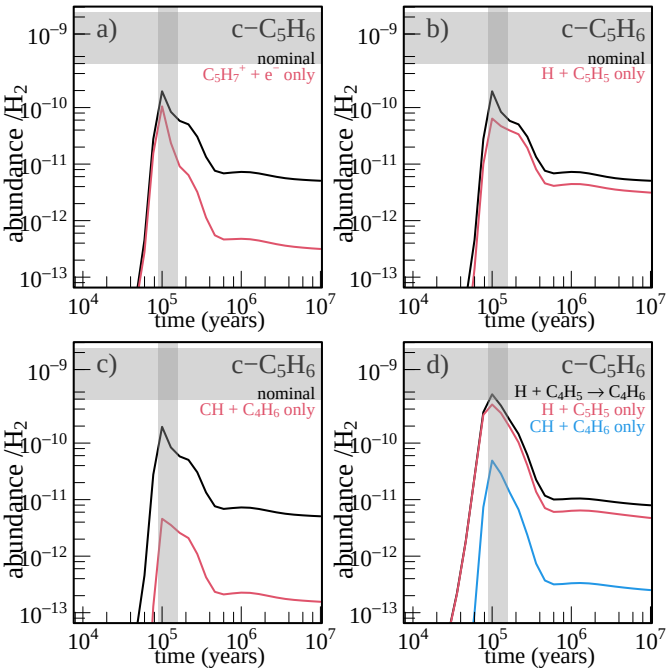

Fig. 3. Gas–grain astrochemical model results for C_5H_6 in dark clouds as a function of cloud age. (a–c) Nominal network results (solid black line); nominal network but with only some specific reactions as a source of C_5H_6 (solid red line). (d) Nominal with $H + C_4H_5$ leading to C_4H_6 (solid black line), nominal with $H + C_4H_5$ leading to C_4H_6 with only $H + C_5H_5$ leading to C_5H_6 (solid red line), and nominal with $H + C_4H_5$ leading to C_4H_6 with only $CH + C_4H_6$ leading to C_5H_6 (solid blue line). The horizontal gray region represents the observed abundances in TMC-1 with an arbitrary error associated (±2).The estimated age of the cloud, marked by a vertical gray region, corresponds to the time at which our model predictions best match the observed abundances of 67 key species.

By contrast, the $O + C_6H_7^+$ reaction does not represent a viable source of $C_5H_7^+$. An activation barrier of approximately 7 kJ mol^{-1} was identified at the M06-2X/AVTZ level in this work. While this level of theory is generally reliable for locating transition states, it is known to underestimate barriers in reactions involving atomic oxygen, which reinforces the conclusion that this pathway is inefficient under dense cloud conditions.

Finally, although many reactions in the network produce $C_5H_5^+$ ions, either as the most stable isomer c−$C_3H_2CHCH_2^+$ or as five-membered-ring structures, these species do not contribute to C_5H_6 formation. The various $C_5H_5^+$ isomers react inefficiently with H_2 (Mallo et al. (2025) and this work), and therefore cannot form $C_5H_7^+$, which excludes them as viable precursors of cyclopentadiene.

4.2. Neutral–neutral chemistry

In addition to ion–molecule processes, C_5H_6 can also be formed through neutral–neutral chemistry. Two such pathways contribute in the model, with the dominant route being the RA reaction $H + C_5H_5$ (48%), and a secondary contribution arising from $CH + C_4H_6$ (4%), as can be seen in Figure 3, panels b and c, respectively.

The $H + C_5H_5$ reaction plays a central role because the C_5H_5 radical is efficiently produced through several channels, most

notably O + C_6H_5 (Frank et al. 1994), and potentially through H-assisted isomerization of $CH_2CHCHCCH$. The latter species is itself efficiently formed via the C + C_4H_6 reaction (Husain & Ioannou 1997; Hahndorf et al. 2000). Rate coefficients for the H + C_5H_5 RA reaction can be estimated from previous experimental and theoretical studies (Frank et al. 1994; Harding et al. 2007; Vuitton et al. 2011). When this pathway is included, the modeled abundance of C_5H_6 is in relatively good agreement with observations, as shown in Figure 3b.

The secondary neutral pathway, CH + C_4H_6, has been investigated previously (He et al. 2020; McCarthy et al. 2021; Cernicharo et al. 2022). In our chemical network, the modeled abundance of CH closely matches observations (Suutarinen et al. 2011). However, C_4H_6 is mainly produced through CH + C_3H_6 (Daugey et al. 2005; Loison & Bergeat 2009; Zhou et al. 2025), with a minor contribution from C + C_3H_7. As a result, the modeled abundance of C_4H_6 remains low, in agreement with Cooke et al. (2023); Agúndez et al. (2025), making CH + C_4H_6 only a minor source of C_5H_6 as shown in Figure 3 c) in contrast to the conclusions of Yang et al. (2024).

If, however, the reaction H + C_4H_5 were to produce C_4H_6 efficiently at the low pressures of dense molecular clouds, at rates approaching those calculated by Harding et al. (2007) for high-pressure conditions, the abundance of C_4H_6 would increase substantially. In that case, the CH + C_4H_6 reaction becomes more important, although it remains a secondary source of C_5H_6. The improved agreement with observations in this scenario primarily arises from the concomitant enhancement of the H + C_5H_5 RA pathway, as higher C_4H_6 abundances also lead to increased production of C_5H_5 isomers, as shown in Figure 3d. However, this scenario also leads to a modeled abundance of $CH_2CHCHCH_2$ of 1.6×10^{-9} at the chemical age of TMC-1, which exceeds the upper limit inferred from the non-detection of C_4H_5CN (Agúndez et al. 2025) by an order of magnitude. For this reason, our nominal model assumes that H + C_4H_5 proceeds exclusively toward CH_3 + C_3H_3, following the ab initio calculations of Lee et al. (2003), despite the high-pressure results of Harding et al. (2007). The importance of the H + C_4H_5 reaction stems from the efficient formation of C_4H_5 radicals (in their various isomeric forms) via C + C_3H_6 (Chastaing et al. 1999; Loison & Bergeat 2004; Chin et al. 2013; Capron et al. 2015).

Finally, the prominence of hydrogen-atom reactions, including RA, is reinforced by the high and nearly constant abundance of atomic hydrogen in dense molecular clouds. Although H atoms readily stick to grains, they are continuously replenished by the cosmic-ray-induced dissociation of H_2. In contrast, heavier atoms such as C, N, and O are efficiently depleted from the gas phase through grain sticking and, in the case of C and O, conversion into CO after $\sim 10^5$ years, further emphasizing the long-term importance of H-driven neutral chemistry.

5. Conclusions

In this work, we revisited the gas-phase chemistry that leads to the formation of cyclopentadiene (C_5H_6) in the cold dark cloud TMC-1 by adopting an integrated strategy that combines new laboratory measurements, quantum chemical calculations, astrochemical modeling, and chemical intuition to guide the identification of the most relevant reaction pathways. In particular, we experimentally characterized the reaction of $C_2H_4^+$ with propyne and allene and incorporated the resulting reaction rate coefficients and branching ratios into an updated chemical network. This synergistic approach allowed us to identify previously underappreciated ion–molecule pathways that contribute to the formation of the key precursor ion $C_5H_7^+$, and to reassess the relative roles of ionic and neutral–neutral chemistry in the synthesis of C_5H_6.

Our updated model partially alleviates the discrepancy between observed and modeled abundances of cyclopentadiene but still reproduces only about 20% of the abundance inferred from observations of TMC-1. Among the ionic routes, the reactions $C_2H_4^+$ + CH_3CCH and $C_3H_7^+$ + C_2H_2 emerge as the dominant sources of $C_5H_7^+$, highlighting the importance of relatively small hydrocarbon ions reacting with abundant unsaturated neutral species. However, even when these channels are treated with experimentally constrained rate coefficients, the overall efficiency of the ion–molecule network remains insufficient to fully account for the observed abundance of C_5H_6.

Neutral–neutral chemistry therefore appears to play a critical complementary role. In our model, the RA reaction H + C_5H_5 is the dominant neutral source of C_5H_6, while the CH + C_4H_6 pathway contributes only marginally under nominal assumptions due to the low modeled abundance of 1,3-butadiene (C_4H_6). The abundance of C_4H_6 remains highly uncertain, as it cannot be directly observed and must be inferred indirectly through chemical proxies whose detections are still debated. Our results suggest that the reaction H + C_4H_5, and more generally hydrogen-atom-driven radiative association processes under low-density interstellar conditions, may represent a key missing ingredient in current chemical networks. Thus, quantifying the efficiency of these reactions at low pressure is essential to further constrain the formation of C_5H_6 and related cyclic hydrocarbons.

More broadly, this study illustrates the strong sensitivity of cyclopentadiene formation to a limited number of chemical pathways that connect linear hydrocarbon chains to the first five-membered ring, even when only a small subset of the associated parameters remains poorly constrained. Resolving the remaining discrepancy between models and observations will therefore require dedicated experimental and theoretical investigations of both the ionic reaction $C_3H_7^+$ + C_2H_2, and neutral radiative association processes involving C_4H_5 and C_5H_5. Improving these constraints is a necessary step toward a coherent description of molecular mass growth from acyclic species to aromatic rings and, ultimately, to larger PAHs and carbonaceous nanostructures in cold interstellar environments.

Acknowledgements. The work was funded by the French "Agence Nationale de la Recherche" (ANR) under grant no. ANR-22-CE29-0013 (Project iSELECTION).This work was also supported by the Programme National "Physique et Chimie du Milieu Interstellaire" (PCMI) and a research grant (VIL71404) from VILLUM FONDEN.

References

Agúndez, M., Cabezas, C., Marcelino, N., et al. 2025, A&A, 697, A82
Anicich, V. G. 2003, JPL Publication-03-19, Pasadena, CA, USA
Anicich, V. G., Wilson, P., & McEwan, M. J. 2003, JACSMAS, 14, 900
Anicich, V. G., Wilson, P. F., & McEwan, M. J. 2006, JACSMS, 17, 544
Bacskay, G. B., & Mackie, J. C. 2001, Phys. Chem. Chem. Phys., 3, 2467
Bouwman, J., Goulay, F., Leone, S. R., & Wilson, K. R. 2012, J. Phys. Chem. A, 116, 3907
Byrne, A. N., Xue, C., Van Voorhis, T., & McGuire, B. A. 2024, PCCP, 26, 26734
Cabezas, C., Agúndez, M., Pérez, C., et al. 2025, A&A, 701, L8
Capron, M., Bourgalais, J., Abhinavam Kailasanathan, R. K., et al. 2015, PCCP, 17, 23833
Caster, K. L., Selby, T. M., Osborn, D. L., Le Picard, S. D., & Goulay, F. 2021, J. Phys. Chem. A, 125, 6927
Cernicharo, J., Agúndez, M., Cabezas, C., et al. 2021a, A&A, 649, L15
Cernicharo, J., Agúndez, M., Kaiser, R. I., et al. 2021b, A&A, 652, L9
Cernicharo, J., Fuentetaja, R., Agúndez, M., et al. 2022, A&A, 663, L9
Cernicharo, J., Cabezas, C., Fuentetaja, R., et al. 2024, A&A, 690, L13

Chastaing, D., James, P., Sims, I., & Smith, I. 1999, PCCP, 1, 2247
Chin, C.-H., Chen, W.-K., Huang, W.-J., Lin, Y.-C., & Lee, S.-H. 2013, Icarus, 222, 254
Cooke, I. R., Xue, C., Changala, P. B., et al. 2023, APJ, 948, 133
Coutens, A., Loison, J.-C., Boulanger, A., et al. 2022, A&A, 660, L6
Cunha De Miranda, B., Romanzin, C., Chefdeville, S., et al. 2015, JPCA, 119, 6082
Daugey, N., Caubet, P., Retail, B., et al. 2005, PCCP, 7, 2921
Dobrijevic, M., Hébrard, E., Loison, J., & Hickson, K. 2014, Icarus, 228, 324
Dobrijevic, M., Loison, J., Hickson, K., & Gronoff, G. 2016, Icarus, 268, 313
Frank, P., Herzler, J., Just, T., & Wahl, C. 1994, in Proceedings of the Combustion Institute, 25 (Elsevier), 833
Frisch, M. J., Trucks, G. W., Schlegel, H. B., et al. 2016, Gaussian~16 Revision C.01, Gaussian Inc., Wallingford, CT
Fuchs, V. R. 1961, Z. Naturforsch., 16a, 1026
Goettl, S. J., He, C., Paul, D., et al. 2022, J. Phys. Chem. A 126, 1889
Hahndorf, I., Lee, H. Y., Mebel, A. M., et al. 2000, J. Chem. Phys., 113, 9622
Haider, N., & Husain, D. 1993, Int. J. Chem. Kinet., 25, 423
Hamberg, M., Vigren, E., Thomas, R., et al. 2011, EAS, 46, 241
Harding, L. B., Klippenstein, S. J., & Georgievskii, Y. 2007, JPCA, 111, 3789
He, C., Zhao, L., Doddipatla, S., et al. 2020, ChemPhysChem, 21, 1295
Hébrard, E., Dobrijevic, M., Loison, J.-C., Bergeat, A., & Hickson, K. 2012, A&A, 541, A21
Hébrard, E., Dobrijevic, M., Loison, J.-C., et al. 2013, A&A, 552, A132
Hickson, K. M., Loison, J.-C., & Wakelam, V. 2021, ACS Earth Space Chem., 5, 824
Hickson, K. M., Loison, J.-C., & Wakelam, V. 2024, ACS Earth Space Chem., 8, 1087
Hincelin, U., Wakelam, V., Hersant, F., et al. 2011, A&A, 530, A61
Hincelin, U., Commerçon, B., Wakelam, V., et al. 2016, APJ, 822, 12
Husain, D., & Ioannou, A. X. 1997, J. Chem. Soc. Faraday Trans., 93, 3625
Knyazev, V. D., & Slagle, I. R. 2001, J. Phys. Chem. A, 105, 3196
Lee, H.-Y., Kislov, V. V., Lin, S.-H., Mebel, A. M., & Neumark, D. M. 2003, Chem. Eur. J., 9, 726
Lifshitz, C., Gleitman, Y., Gefen, S., Shainok, U., & Dotan, I. 1981, IJMS, 40, 1
Loison, J. C., & Bergeat, A. 2004, Phys. Chem. Chem. Phys., 6, 5396
Loison, J.-C., & Bergeat, A. 2009, Phys. Chem. Chem. Phys., 11, 655
Loison, J.-C., Wakelam, V., Hickson, K. M., Bergeat, A., & Mereau, R. 2013, MNRAS, 437, 930
Loison, J.-C., Wakelam, V., & Hickson, K. M. 2014, MNRAS, 443, 398
Loison, J., Hébrard, E., Dobrijevic, M., et al. 2015, Icarus, 247, 218
Loison, J.-C., Agúndez, M., Marcelino, N., et al. 2016, MNRAS, 456, 4101
Loison, J.-C., Agúndez, M., Wakelam, V., et al. 2017, MNRAS, 470, 4075
Loison, J., Dobrijevic, M., & Hickson, K. 2019, Icarus, 329, 55
Loison, J.-C., Rossi, C., Solem, N., et al. 2026, Nat. Astron., under review, [arXiv:2506.13290]
Loru, D., Cabezas, C., Cernicharo, J., Schnell, M., & Steber, A. L. 2023, A&A, 677, A166
Mallo, M., Agúndez, M., Cernicharo, J., & Molpeceres, G. 2025, A&A, 704, A249
Manigand, S., Coutens, A., Loison, J.-C., et al. 2021, A&A, 645, A53
McCarthy, M. C., Lee, K. L. K., Loomis, R. A., et al. 2021, Nat. Astron., 5, 176
McEwan, Murray, J., Scott, Graham, B. I., Adams, Nigel, G., et al. 1999, ApJ, 513, 287
McEwan, M. J., & Anicich, V. G. 2007, Mass Spectrom. Rev., 26, 281
McEwan, M. J., Scott, G. B., & Anicich, V. G. 1998, IJMS, 172, 209
McGuire, B. A., Burkhardt, A. M., Kalenskii, S., et al. 2018, Science, 359, 202
McGuire, B. A., Loomis, R. A., Burkhardt, A. M., et al. 2021, Science, 371, 1265
Mu, X., Lu, I. C., Lee, S.-H., Wang, X., & Yang, X. 2004, J. Chem. Phys., 121, 4684
Newby, J. J., Stearns, J. A., Liu, C.-P., & Zwier, T. S. 2007, J. Phys. Chem. A, 111, 10914
Petrie, S., Javahery, G., & Bohme, D. K. 1992, J. Am. Chem. Soc., 114, 9205
Rossi, C., Alcaraz, C., Thissen, R., & Jacovella, U. 2023, J. Phys. Org. Chem., 36, e4489
Rossi, C., Muller, G., Solem, N., et al. 2025, ACS Earth Space Chem. 9, 349
Roy, K., Horn, C., Frank, P., Slutsky, V. G., & Just, T. 1998, Symp. (Int.) Combust., 27, 329
Ruaud, M., Wakelam, V., & Hersant, F. 2016, MNRAS, 459, 3756
Scott, G. B. I., Milligan, D. B., Fairley, D. A., Freeman, C. G., & McEwan, M. J. 2000, J. Chem. Phys., 112, 4959
Sita, M. L., Changala, P. B., Xue, C., et al. 2022, Astrophys. J., 938, L12
Smith, R. D., & Futrell, J. H. 1978, Int. J. Mass Spectrom. Ion Phys., 26, 111
Smyth, K. C., G., L. S., & Ausloos, P. 1982, Combust. Sci. Technol., 28, 147
Snow, T. P., Le Page, V., Keheyan, Y., & Bierbaum, V. M. 1998, Nature, 391, 259
Suutarinen, A., Geppert, W. D., Harju, J., et al. 2011, A&A, 531, A121
Thaddeus, P., Vrtilek, J., & Gottlieb, C. 1985, Astrophys. J., 299, L63
Vuitton, V., Yelle, R., Lavvas, P., & Klippenstein, S. 2011, APJ, 744, 11
Wakelam, V., Ruaud, M., Gratier, P., & Bonnell, I. 2019, MNRAS, 486, 4198
Wakelam, V., Dartois, E., Chabot, M., et al. 2021, A&A, 652, A63
Wakelam, V., Gratier, P., Loison, J.-C., et al. 2024, A&A, 689, A63
Wenzel, G., Cooke, I. R., Changala, P. B., et al. 2024, Science, 386, 810
Wenzel, G., Gong, S., Xue, C., et al. 2025, Astrophys. J., 984, L36
Yang, Z., Medvedkov, I. A., Goettl, S. J., et al. 2024, PNAS, 121, e2409933121
Zhao, Y., & Truhlar, D. G. 2008, Theor. Chem. Acc., 120, 215
Zhou, F., Ma, S., Li, L., et al. 2025, JCP, 162, 9

Appendix A: Elemental abundances and other model parameters

Table A.1. Elemental abundances and other model parameters

Element	Abundance[a]	$n_H + 2n_{H_2}$ (cm^{-3})	T (K)	Cosmic ray ionization rate (s^{-1})	A_V
H_2	0.5	1.0×10^5	10	1.3×10^{-17}	10
He	0.09				
C^+	1.4×10^{-4}				
N	3.0×10^{-5}				
O	1.4×10^{-4}				
s-H_2O[b]	1.0×10^{-4}				
S^+	4.0×10^{-6}				
Fe^+	2.0×10^{-8}				
Cl^+	1.0×10^{-7}				
F	6.7×10^{-9}				

[a] Relative to total hydrogen ($n_H + 2n_{H_2}$).
[b] s-H_2O denotes H_2O on grain surfaces.

Appendix B: $C_2H_4^+ + C_3H_4$ reactions including secondary products

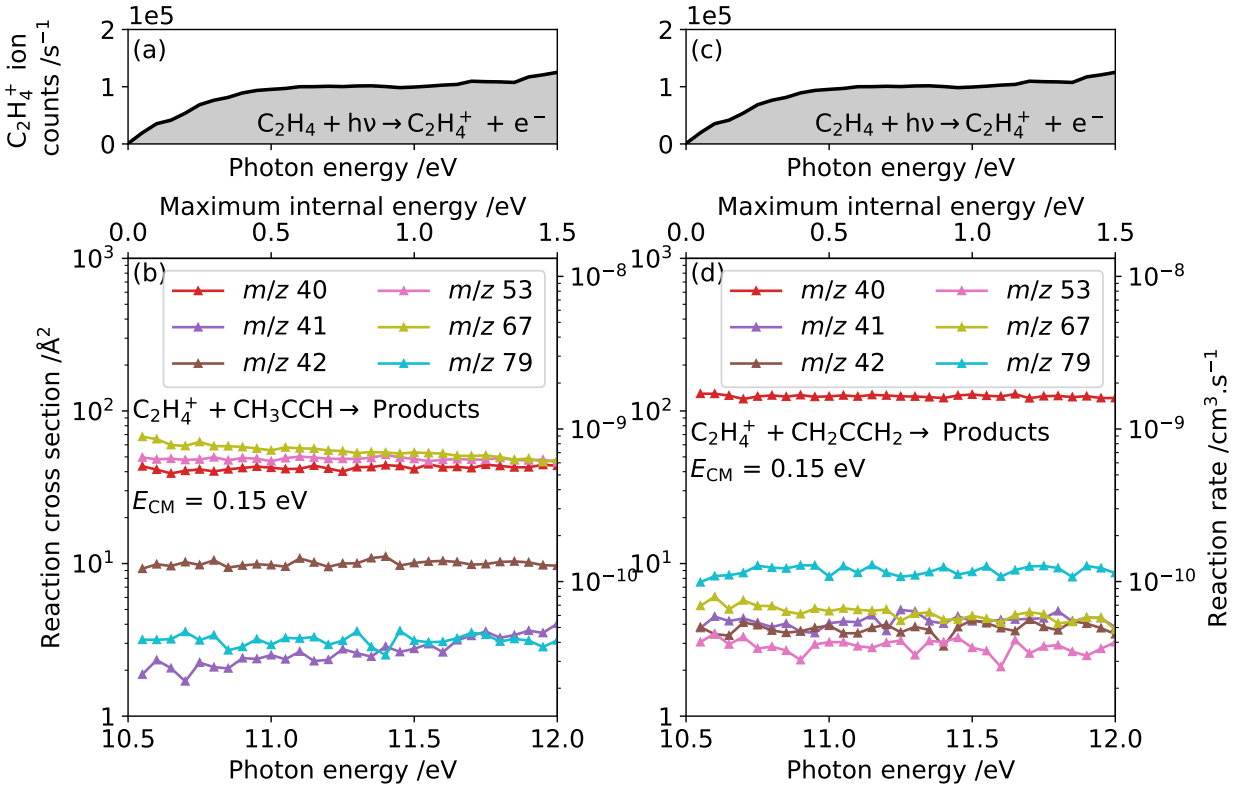

Fig. B.1. Panels a and c display the $C_2H_4^+$ parent-ion signal from the photoionization of ethylene. Panels b and d show the reaction cross sections (left axis) and rate constants (right axis) with propyne and allene, respectively, as a function of photon energy.

Appendix C: Chemical network used for the model

Table C.1. Chemical network used for the model. Rate coefficients $\alpha(T/300)^{\beta}\exp(-\gamma/T)$ are in units of $cm^3\,s^{-1}$. ΔH_R in $kJ\,mol^{-1}$. Reactions highlighted in grey such as 15 are not included in the network.

#	Reaction	ΔH_R	α	β	γ	ref
1	$H_3^+ + C_5H_5 \rightarrow C_5H_6^+ + H_2$	-407	2.0E-09	-0.5	0	Typical rate constant for H_3^+ reaction with hydrocarbon Anicich (2003)
2	$H_3^+ + C_5H_6 \rightarrow C_5H_7^+ + H_2$	-395	2.0E-09	-0.5	0	Typical rate constant for H_3^+ reaction with hydrocarbon Anicich (2003)
3	$C^+ + C_5H_6 \rightarrow C + C_5H_6^+$		2.4E-09	0	0	Branching ratio from Smith & Futrell (1978) rate equal to $C^+ + C_6H_6$
4	$CH_3^+ + CH_2CHCHCH_2 \rightarrow C_5H_7^+ + H_2$	-366	3.0E-10	0	0	Approximate guessed branching ratios.
	$C_2H_5^+ + CH_3CCH$	-123	3.0E-10	0	0	
	$C_2H_3^+ + C_3H_6$	-73	3.0E-10	0	0	
5	$C_2H_3^+ + C_3H_6 \rightarrow C_5H_7^+ + H_2$	-293	1.0E-10	-0.5	0	
	$CH_2CHCCH_2^+ + CH_4$	-166	0			One very old study, Fuchs (1961)
	$CH_3CCCH_2^+ + CH_4$	-138	2.0E-10	-0.5	0	leading to $C_4H_5^+ + CH_4$ only which is a
	$CH_3CHCCH^+ + CH_4$	-122	0			strange result considering the $C_2H_3^+$ +
	$C_3H_5^+ + C_2H_4$	-122	5.0E-10	-0.5	0	c-C_3H_6 reaction which leads to $C_3H_5^+$ +
	$C_3H_7^+ + C_2H_2$	-73	2.0E-10	-0.5	0	C_2H_4 and $C_3H_7^+ + C_2H_2$.
	$c{-}C_5H_8^+ + H$	-26	0			
6	$C_2H_4^+ + CH_3CCH \rightarrow C_5H_7^+ + H$	-176	1.0E-09	-0.5	0	This work and Anicich et al. (2006)
	$C_4H_5^+ + CH_3$	-47	6.0E-10	-0.5	0	
	$C_3H_6^+ + C_2H_2$	-59	1.2E-10	-0.5	0	
	$C_3H_5^+ + C_2H_3$	+18	0			
	$CH_3CCH^+ + C_2H_4$	-8	5.0E-10	-0.5	0	
7	$C_2H_4^+ + CH_2CCH_2 \rightarrow C_5H_7^+ + H$	-176	7.0E-11	0	0	This work
	$C_4H_5^+ + CH_3$	-47	0			
	$C_3H_6^+ + C_2H_2$	-59	0			
	$C_3H_5^+ + C_2H_3$	+18	0			
	$CH_2CCH_2^+ + C_2H_4$	-65	1.1E-09	0	0	
8	$C_2H_5^+ + CH_3CCH \rightarrow C_5H_7^+ + H_2$	-243	2.0E-10	-0.5	0	Rate equal to 1.1E-09 Lifshitz et al.
	$CH_3CCCH_2^+ + CH_4$	-89	2.0E-10	-0.5	0	(1981). Approximate guessed branching
	$C_3H_5^+ + C_2H_4$	-72	7.0E-10	-0.5	0	ratios
	$C_3H_7^+ + C_2H_2$	-56	0			
9	$C_2H_5^+ + CH_2CCH_2 \rightarrow C_5H_7^+ + H_2$	-243	4.0E-10	0	0	Rate equal to 1.1E-09 Lifshitz et al.
	$CH_3CCCH_2^+ + CH_4$	-89	4.0E-10	0	0	(1981). Approximate guessed branching
	$C_3H_5^+ + C_2H_4$	-72	1.6E-09	0	0	ratios
	$C_3H_7^+ + C_2H_2$	-56	0			
10	$l{-}C_3H_3^+ + C_2H_4 \rightarrow C_5H_7^+ + h\nu$	-405	0			Mallo et al. (2025); Smyth et al. (1982)
	$C_5H_6^+ + H$	-82	0			
	$c{-}C_5H_5^+ + H_2$	-169	1.0E-10	0	0	
	$C_3H_5^+ + C_2H_2$	-63	0			
	$CH_3CCH_2^+ + C_2H_2$	-46	1.0E-09	0	0	
11	$C_3H_4^+ + C_2H_4 \rightarrow C_5H_7^+ + H$	-111	7.4E-10	0	0	McEwan & Anicich (2007). Older
	$C_4H_5^+ + CH_3$	-64	9.0E-11	0	0	values from Anicich et al. (2006) are slightly different. $C_4H_5^+$: c-$C_3H_2CH_3^+$
12	$C_3H_5^+ + C_2H_4 \rightarrow C_5H_7^+ + H_2$	-171	1.2E-10	0	0	McEwan et al. (1998). Others values: 7.7E-11 Anicich et al. (2003), 8.9E-11 Anicich et al. (2006)
13	$C_3H_6^+ + C_2H_2 \rightarrow C_5H_7^+ + H$	-117	7.4E-10	0	0	[a]
	$C_4H_5^+ + CH_3$	-72	9.0E-11	0	0	
14	$C_3H_7^+ + C_2H_2 \rightarrow c{-}C_5H_9^+ + h\nu$	-211	0			[b]
	$C_5H_7^+ + H_2$	-187	5.0E-10	0	0	
	$c{-}C_5H_8^+ + H$	+80	0			
15	$C_4H_2^+ + C_3H_6 \rightarrow C_7H_7^+ + H$	-355				Likely not a source of $C_5H_7^+$
	$C_5H_6^+ + C_2H_2$	-268				
16	$C_4H_3^+ + CH_4 \rightarrow C_5H_7^+$	-347				Entrance barrier equal to +26 kJ/mol Mallo et al. (2025)

Table C.1. Ccontinued.

#	Reaction	ΔH_R	α	β	γ	ref
17	$C_4H_3^+ + C_3H_6 \rightarrow C_6H_5CH_3^+ + H$	-175				Potential (minor) source of $C_5H_7^+$ but requires further investigation
	$C_5H_7^+ + C_2H_2$	-214				
	$C_5H_5^+ + C_2H_4$	-150				
18	$C_4H_4^+ + CH_4 \rightarrow C_5H_7^+ + H$	-70				Entrance barrier equal to +38 kJ/mol Mallo et al. (2025) for CH_2CHCCH^+ isomer
19	$C_4H_5^+ + CH_4 \rightarrow C_5H_7^+ + H_2$	-127				Likely a barrier in the entrance valley
20	$C_5H_5^+ + H_2 \rightarrow C_5H_7^+ + h\nu$	-235				Large entrance barrier Mallo et al. (2025)
21	$C_5H_6^+ + H \rightarrow C_5H_7^+ + h\nu$	-323	1.0E-11	-0.5	0	/ H + $C_6H_6^+$ Snow et al. (1998); Petrie et al. (1992)
	$C_5H_5^+ + H_2$	-88	0			
22	$C_5H_6^+ + O \rightarrow C_4H_6^+ + CO$	-339	1.0E-10	0	0	Scott et al. (2000)
23	$C_5H_6^+ + H_2 \rightarrow C_5H_8^+$	-57				Very large entrance barrier at M06-2X/AVTZ level (this work)
	$C_5H_7^+ + H$	+102				
24	$C_6H_6^+ + N \rightarrow C_5H_5^+ + HCN$	-229	1.4E-10	0	0	McEwan et al. (1999)
25	$C_6H_6^+ + O \rightarrow C_5H_6^+ + CO$	-376	9.5E-11	0	0	Snow et al. (1998); Scott et al. (2000)
	$C_4H_4O^+ + C_2H_2$		1.0E-11	0	0	
26	$HCO^+ + C_5H_5 \rightarrow C_5H_6^+ + CO$	-264	1.0E-09	0	0	Capture rate theory
27	$HCO^+ + C_5H_6 \rightarrow C_5H_7^+ + CO$	-252	1.0E-09	0	0	Capture rate theory
28	$H + C_4H_5 \rightarrow C_4H_6 + h\nu$	-418	0			Harding et al. (2007). Branching ratio deduced from C_4H_6 photodissociation Mu et al. (2004); Newby et al. (2007); Lee et al. (2003)
	$CH_3 + C_3H_3$	-41	2.0E-10	0	0	
	$H_2C_2 + C_2H_4$	-50	0			
29	$H + l\text{–}C_5H_5 \rightarrow C_5H_5 + H$	-118	1.0E-10	0	0	[c]
	$CH_3CCH + C_2H_2$	-183	2.0E-11	0	0	
	$CH_2CCH_2 + C_2H_2$	-183	8.0E-11	0	0	
30	$H + C_5H_5 \rightarrow C_5H_6 + h\nu$	-335	2.0E-10	0	0	Deduced from high pressure rate constant Harding et al. (2007). Value for T=10K. The TS toward the bimolecular channel are above the entrance energy Bacskay & Mackie (2001)
	$CH_3C_4H + H_2$	-77	0			
	$CH_3CCH + C_2H_2$	-66	0			
	$CH_2CCH_2 + C_2H_2$	-66	0			
31	$C + C_3H_6 \rightarrow CH_3 + C_3H_3$	-246	1.5e-10	0	0	Chastaing et al. (1999); Loison & Bergeat (2004); Chin et al. (2013); Capron et al. (2015)
	$H + C_4H_5$	-212	1.5e-10	0	0	
32	$C + CH_2CHCHCH_2 \rightarrow l\text{–}C_5H_5 + H$	-233	3.6e-10	0	0	Rate from Husain & Ioannou (1997) (with a smaller value), branching ratio from Hahndorf et al. (2000)
	$C_2H_3 + C_3H_3$	-189	4.0e-11	0	0	
33	$C + C_5H_5 \rightarrow C_6H_4 + H$	-292	4.0E-10	0	0	/ $C + C_5H_6$
	$C_2H_3C_4H + H$	-257	0			
	$HCCCHCHCCH + H$	-245	0			
34	$C + C_5H_6 \rightarrow C_6H_5 + H$	-312	4.0E-10	0	0	Haider & Husain (1993) (with lower rate)
35	$CH + CH_2CHCHCH_2 \rightarrow C_5H_6 + H$	-354	4.0E-10	0	0	He et al. (2020); McCarthy et al. (2021); Cernicharo et al. (2022)
36	$CH + C_5H_6 \rightarrow C_6H_6 + H$	-439	4.0e-10	0	0	Products from Caster et al. (2021)
37	$CH_2 + C_4H_5 \rightarrow C_5H_6 + H$	-323				[d]
	$C_2H_3C_2H + CH_3$	-244				
	$C_3H_3 + C_2H_4$	-275				
	$C_3H_5 + C_2H_2$	-277				
38	$CH_3 + C_3H_3 \rightarrow C_4H_6 + h\nu$	-372	1.0e-10	0	0	Deduced from high pressure rate constant Knyazev & Slagle (2001). Value for T=10K only.

Table C.1. Ccontinued.

#	Reaction	ΔH_R	α	β	γ	ref
39	$CH_3 + C_4H_3 \rightarrow C_5H_6$	-485				We do not consider this reaction which likely produces little to no cyclopentadiene since it requires multiple isomerization and a complex pathway.
	$C_5H_5 + H$	-149				
	$C_4H_2 + CH_4$	-246				
	$C_3H_3 + C_2H_3$	-2				
	$C_3H_2 + C_2H_4$	-25				
40	$C_2H + C_3H_6 \rightarrow C_2H_3C_2H + CH_3$	-156	1.0E-10	0	0	Bouwman et al. (2012); Goettl et al. (2022)
	$l\text{-}C_5H_6 + H$	-120	1.0E-10	0	0	
	$C_5H_6 + H$	-238	0			
41	$C_2H_3 + C_3H_3 \rightarrow CH_2CHCHCCH + H$	-43	1.0E-11	0	0	[e]
	$CH_2CHCCCH_2 + H$	-36	1.0E-11			
	$C_5H_5 + H$	-161	3.0E-11			
42	$N + C_5H_5 \rightarrow C_2H_3C_2H + HCN$	-311	6.0E-11	0	0	/ N + radical reactions
43	$O + C_5H_5 \rightarrow c\text{-}C_5H_4O + H$	-232	1.1E-10	0	0	Frank et al. (1994)
	$C_2H_3C_2H + HCO$	-181	0			
	$C_4H_5 + CO$	-310	0			
44	$O + C_6H_5 \rightarrow C_5H_5 + CO$	-420	1.1E-10	0	0	Frank et al. (1994)
45	$C_5H_6^+ + e^- \rightarrow C_5H_5 + H$	-476	1.0E-06	-0.3	0	By comparison with similar reactions.
	$CH_3CCH + C_2H_2$	-542	5.0E-07	-0.3	0	
	$CH_2CCH_2 + C_2H_2$	-542	5.0E-07	-0.3	0	
46	$C_5H_7^+ + e^- \rightarrow C_5H_6 + H$	-488	2.0E-06	-0.3	0	See text.
	$C_2H_3C_2H + CH_3$	-409	0			
	$CH_2CCCH_2^+ + CH_3$	-409	0			

[a] The $C_3H_6^+ + C_2H_2$ reaction is a potential source of $C_5H_7^+$, but it must be a minor source since $C_3H_6^+$ is not very abundant. We use the same rates as for the iso-electronic reaction $C_3H_4^+ + C_2H_4$.

[b] There are two isomers for $C_3H_7^+$: $CH_3CHCH_3^+$ (the most stable) and $CH_3CH_2CH_2^+$ (+52 kJ/mol) separated by TS a localized +85 kJ/mol above $CH_3CHCH_3^+$. Both isomers should exist in dense molecular cloud. We conducted preliminary calculations showing that the isomer $CH_3CH_2CH_2^+$ reacts with C_2H_2 to produce $C_5H_7^+ + H_2$. Further study is needed, but this reaction is likely an important pathway for the production of C_5H_6, as both $C_3H_7^+$ and C_2H_2 are fairly abundant in the model.

[c] $l\text{-}C_5H_5$ (several mesomeric forms: $H_2C{=}CH{-}CH{-}CC{-}H \leftrightarrow H_2C{=}CH{-}CH{=}C{=}C{-}H \leftrightarrow H_2C{-}CH{=}CH{-}CC{-}H$) is produced by $C + CH_2CHCHCH_2$ and will react without a barrier on the singlet surface (doublet-doublet reaction) to yield $H_2C{=}CH{-}CH_2{-}CC{-}H$ (likely the main product as $H_2C{=}CH{-}CH{-}CC{-}H$ is the most stable configuration), $H_2C{=}CH{-}CH{=}C{=}CH_2$ and $CH_3{-}CH{=}CH{-}CC{-}H$. $H_2C{=}CH{-}CH_2{-}CC{-}H$ can lead to $c\text{-}C_5H_6$ through a TS localized -84 kJ/mol below the $H + l\text{-}C_5H_5$ entrance level and then to $C_5H_5 + H$ (without exit TS), or to $CH_2CCH_2 + C_2H_2$ through a TS localized -65 kJ/mol below the $H + l\text{-}C_5H_5$ entrance level Bacskay & Mackie (2001). The TS involved have similar energies and structures and then $H_2C{=}CH{-}CH_2{-}CC{-}H$ should lead to $H + c\text{-}C_5H_5$ and $CH_2CCH_2 + C_2H_2$ in a similar amount. $H_2C{=}CH{-}CH{=}C{=}CH_2$ can lead to $c\text{-}C_5H_6$ through a TS localized -144 kJ/mol below the $H + l\text{-}C_5H_5$ entrance level and then to $C_5H_5 + H$ (without exit TS) or to $CH_2CCH_2 + C_2H_2$ through a TS localized -77 kJ/mol below the $H + l\text{-}C_5H_5$ entrance level Bacskay & Mackie (2001). So $H_2C{=}CH{-}CH{=}C{=}CH_2$ should lead mainly to $H + c\text{-}C_5H_5$. The preferential production of $c\text{-}C_5H_5$ is also observed during the pyrolysis of $c\text{-}C_5H_6$ Bacskay & Mackie (2001); Roy et al. (1998). Further studies on this reaction will be necessary to obtain more accurate rates for this important reaction for $c\text{-}C_5H_6$ modeling in interstellar media.

[d] The reaction $CH_2 + C_4H_5 \rightarrow C_5H_6 + H$ is most certainly rapid at low temperatures as radical-radical reaction. The first step of this reaction is the formation of the linear C_5H_7 adduct. There are several isomers of C_4H_5 produced in the network through mostly through the $C + C_3H_6$ reaction Chastaing et al. (1999); Loison & Bergeat (2004); Chin et al. (2013); Capron et al. (2015) and for the most stable one, CH_3CCCH_2, multiple mesomeric forms exist, leading to the possible production of a large number of C_5H_7 isomers. The production of $c\text{-}C_5H_6$ may be possible but would require numerous isomerization of the initial C_5H_7 adducts and is likely unfavored. Moreover, even though the reactants are produced by efficient reactions, they react with atoms (H, C, O, and N) without a barrier and have relatively low concentrations in dense clouds, limiting the significance of this reaction. Nevertheless, we performed a run assuming a rate of 1×10^{-10} cm^3 s^{-1} for the $CH_2 + C_4H_5 \rightarrow C_5H_6 + H$ reaction as a test and thus showing that this reaction is negligible under dense cloud conditions.

[e] The first step is CH_2CHCH_2CCH and $CH_2CHCHCCH_2$ formation without barrier (radical-radical association). The TS for $CH_2CHCH_2CCH \rightarrow CH_2CHCHCCH_2$ is located -63 kJ/mol below $C_2H_3 + C_3H_3$. The TS for $CH_2CHCHCCH_2 \rightarrow CH_2CHCHCHCH$ is located -115 kJ/mol below the entrance level and it seems that there is no, or very low, barrier for $CH_2CHCHCHCH$ cyclisation toward C_5H_6.